

# A Compact High Gain Circular Shaped Two-Port MIMO Antenna with Fractal DGS for Downlink Satellite Communication

Manjula Sanugomula and Ketavath Kumar Naik\*

*Antenna Research Laboratory, Department of Electronics and Communication Engineering  
Koneru Lakshmaiah Education Foundation (KLEF) deemed to be University, Vaddeswaram, Guntur-522502, India*

**ABSTRACT:** This paper presents an innovative high-gain multiple-input-multiple-output (MIMO) antenna featuring a compact circular shape, enhanced by strategically positioned slots, slits, and defected grounds created by etching multiple iterations of a circle inserted with a triangle shape. The investigation thoroughly explores the various traits and properties exhibited by the antenna. The antenna design harmoniously incorporates two radiating elements shaped in circles, positioned 16 mm apart from their centers, and has been physically constructed using an FR4 substrate. Enhancing the antenna's bandwidth and gain requires the implementation of slots with fractal patterns on the ground with a precise edge-to-edge separation of 2.5 mm. The placement of the antenna elements at a 16 mm distance guarantees an isolation level exceeding 15 dB consistently throughout the entire wideband frequency range. The dimensions of the compact MIMO antenna are tailored to be  $1.12\lambda \times 1.8\lambda \times 0.091\lambda$  ( $20 \times 32 \times 1.62 \text{ mm}^3$ ). In this study, the circular patch MIMO antenna with a fractal defected ground structure (DGS) resonates precisely at 16.903 GHz. It showcases an impressive impedance bandwidth spanning 2.027 GHz, ranging from 15.946 GHz to 17.973 GHz. It exhibits a reflection coefficient of  $-43.82 \text{ dB}$  and achieves an observed gain of 6.25 dBi. The observed results include a minimal envelope correlation coefficient ( $< 0.025$ ) and a substantial diversity gain ( $> 9.89$ ). The measured results mirror the simulated outcomes, affirming the effectiveness of the wideband, high-gain antenna design. Its bandwidth and gain are well-suited for satellite communications, particularly in downlink applications, enabling faster data transmission rates.

## 1. INTRODUCTION

Antennas in today's wireless communication systems must be both compact and smart, especially for satellite applications. Microstrip patch antennas offer benefits such as minimal profile, compact size, lightweight design [1], and seamless integration into high-frequency systems. When designing antennas for satellite applications, prioritizing size and ease of installation become crucial. These antennas highlight higher reflection coefficients and extensive bandwidth parameters as their primary focus [2]. However, patch antennas inherently exhibit a limited impedance bandwidth and lower gain [3]. The patch antenna structure is responsible for achieving parameters. A circular patch antenna helps to get a wider bandwidth compared to other structures [4]. In response to these challenges, several approaches have been recommended, including substrate electrical thickening, incorporating slots on the patch, and employing defected ground structures (DGS) [5]. In general, employing fractal patterns as patches or slots in antennas has the effect of reducing their physical dimensions and generating a multiband response in their resonant properties [6]. For multiple band generation, Y-shaped and rectangular concentric MIMO patch antennas are designed [7]. A DGS is utilized for super wide-band with stepped-meander-lines [8] for ultra-wideband (UWB) applications. A UWB band-pass-filter (BPF) with tunable-notch is designed with a DGS antenna [9].

The introduction of MIMO technology strives to mitigate the challenges posed by multipath fading while simultaneously

improving the transmission quality within communication systems [10]. Multiband with wide impedance bandwidth is possible with a fractal structure over a patch [11]. For wireless applications, high gain with enhanced antennas is required [12]. Considering the multiple antennas in MIMO, compactness decreases [13, 14]. Satellite and Ku band applications require compact antennas with high gain and wide bandwidth [15]. Creating slits and slots on the radiators and ground serves to reduce the mutual interference between neighboring antennas [16]. Creating a wide slot over a patch helps to get wider bandwidth [17]. A circle-shaped microstrip patch antenna fed by microstrip feeding helps in achieving wider bandwidth [18]. Placing dual elements as patches also improves the bandwidth [19]. Enhancement of gain without compromising bandwidth is essential in communications. Creating concentric circular ring slots [20] and cavity-backed slot antenna [21] provides high gain with wide bandwidth. A compact circular MIMO antenna design is suitable for UWB applications with appreciable radiation characteristics [22, 23]. This paper presents a concise, circular, two-port MIMO antenna design featuring slits and slots on the patch, along with circular and triangle fractals at the ground to enhance gain of different MIMO antennas in 5G systems [24]. Different circular shape MIMO antennas are proposed for WLAN and wireless applications [25].

The proposed antenna extends the bandwidth from 15.946 GHz to 17.973 GHz, and a reflection coefficient ( $S_{11} = S_{22}$ ) of  $-43.82 \text{ dB}$  is observed. Etching the slits facilitated enhanced gain characteristics, while the MIMO concept effectively mitigated multi-path fading, leading to

\* Corresponding author: Ketavath Kumar Naik (drkumarkn@hotmail.com).

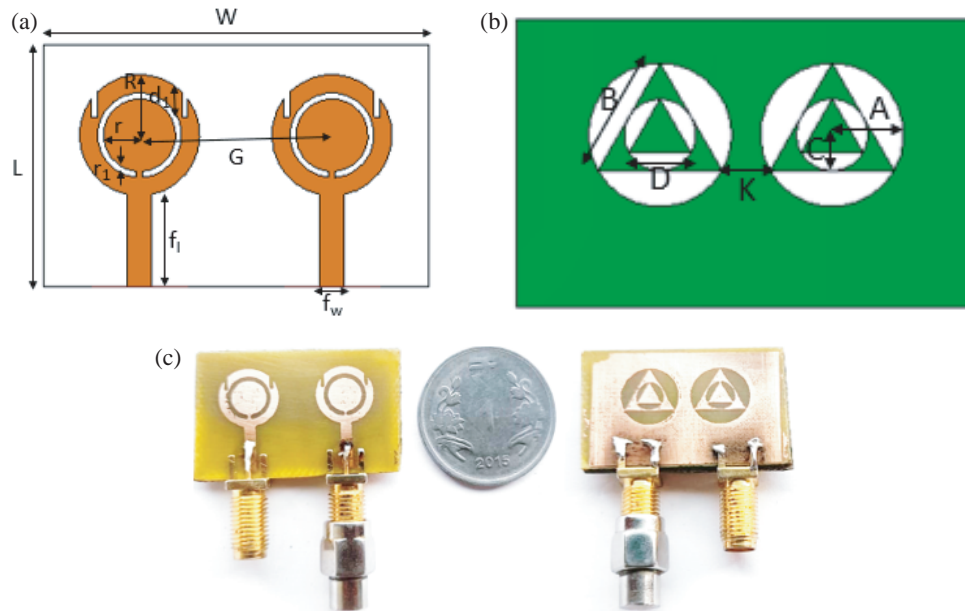


**FIGURE 1.** (a) Top View of the Proposed MIMO Antenna. (b) Bottom View-Ground with fractal DGS. (c) Fabricated Prototype.

reduced interference. At its resonant frequency of 16.903 GHz, the antenna achieves a gain of 6.25 dBi. The remarkable coherence between the simulated and measured outcomes validates the designed antenna as the prime choice for satellite communication applications.

The paper is structured into three main sections. Section 2 presents the antenna design along with its parametric analysis. Section 3 provides the simulation results, and Section 4 offers the conclusion.

## 2. ANTENNA DESIGN

The fundamental structure of the microstrip patch antenna includes vital elements: a substrate plane, a ground plane, a microstrip feed, and a versatile patch, which can take on various shapes such as ellipse, circle, rectangle, and beyond. We designed a microstrip patch antenna featuring a circular shape, crafting it from copper material on an FR4 substrate for enhanced performance and efficiency. After rectangular patch antenna, circular patch antenna emerges as another widely favored geometry among microstrip antennas, valued for its relatively compact dimensions. In this suggested design, ‘ $t_s$ ’ represents the substrate’s thickness. The resonating frequency of the circular patch antenna is determined using the following expression (1).

$$f_r = \frac{8.794}{r_e \sqrt{\epsilon_r}} \quad (1)$$

where  $f_r$  is the resonant frequency of the patch,  $\epsilon_r$  the relative permittivity of the substrate, and  $r_e$  the effective radius of the circular patch given by [1]

$$r_e = R \left[ 1 + \frac{2h}{\pi R \epsilon_r} \left\{ \ln \left( \frac{R}{2h} \right) + (1.41 \epsilon_r + 1.77) \right\} \right]^{\frac{1}{2}} \quad (2)$$

where  $R$  is the radius of the circular patch and  $h$  the height of the substrate.

Figure 1 illustrates the setup of the proposed two-port MIMO antenna. Fig. 1(a) displays the antenna’s top view, while Fig. 1(b) provides the bottom view for a comprehensive understanding of its configuration. The antenna is constructed on a commercially available substrate of FR-4 with a dielectric constant  $\epsilon_r$  of 4.3, a loss tangent of 0.025, and a thickness of 1.6 mm. A width of 7.5 mm is chosen for the feed lines of both elements to guarantee a line characteristic impedance of  $50 \Omega$ , ensuring optimal performance and compatibility.

The etched ground is incorporated to enhance stopband reduction by altering the distribution of ground currents. This strategy minimizes the creation of multiple frequency bands, thereby amplifying the overall antenna performance. The antenna comprises a circular radiating element intricately designed with slits and slots, accompanied by a defective ground structure. This ground structure combines circle and triangle shapes in fractal patterns across three iterations. Fig. 1(c) presents the fabricated prototype of the proposed two-port MIMO antenna. Table 1 tabulates the optimized parameters of the designed two-port MIMO antenna.

### 2.1. Evaluation of the Two-Port MIMO Antenna Design

Figs. 2(a)–(e) illustrate the successive phases in the development of the proposed antenna, specifically tailored for the two-port element. Initially, Ant. 1 was developed as a basic circle-shaped radiator that was crafted with full ground, shown in Fig. 2(a), and simulated to achieve a reflection coefficient of  $-28.5$  dB at a resonating frequency of 17.72 GHz. Subsequently, alterations were made by etching a circular slot with

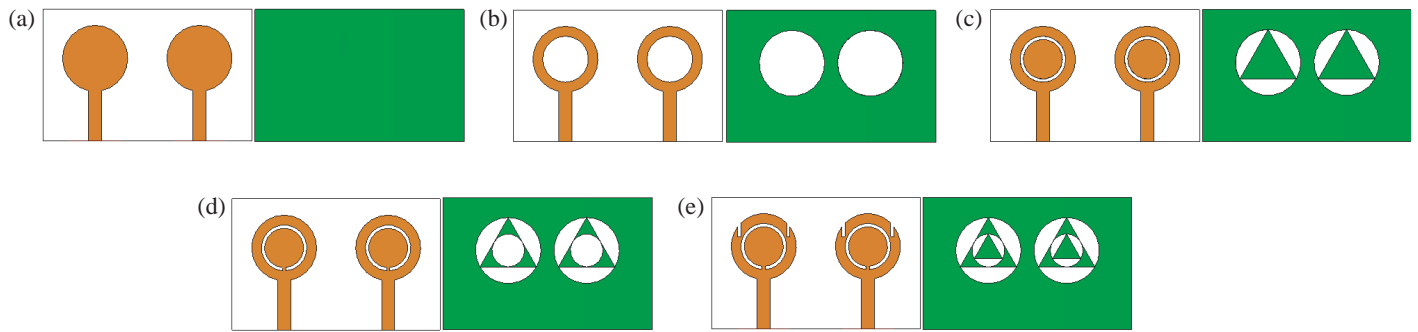


FIGURE 2. (a) Ant. 1, (b) Ant. 2, (c) Ant. 3, (d) Ant. 4, (e) Ant. 5 Proposed design.

TABLE 1. Dimensions of the optimized parameters for the proposed antenna.

Parameter	Dimensions (mm)	Parameter	Dimensions (mm)
$L$	20.0	$d_1$	3.5
$W$	32.0	$G$	16.0
$f_l$	7.5	$A$	5.0
$f_w$	2.0	$B$	8.6
$R$	5.0	$C$	2.5
$r_1$	0.5	$D$	4.3
$r$	3.0	$K$	3.0

a radius of 3.5 mm over the patch and two circular slots with a radius of 5 mm over the ground in Ant. 2 and shown in Fig. 2(b). This adjustment resulted in a gain value of 5.7 dBi and an improvement in bandwidth by 300 MHz compared to the previous iteration. The antenna parameters at different operating frequencies concern different stages of antenna design.

Continuing the refinement process, Ant. 3 was developed by introducing a circle into the etched slot and a triangle into the grounded slot in Ant. 2 to increase the conducting area, which helps to improve the reflection coefficient, and it is presented in Fig. 2(c). This adjustment resulted in an enhanced reflection coefficient of  $-52.03$  dB without compromising the bandwidth, but a reduction in gain of 0.5 dB compared to the previous design. In pursuit of higher gain and broader bandwidth, we created a path to alter the current direction at the patch level and created slots within the triangle over the ground in the design of Ant. 4, shown in Fig. 2(d). With this gain parameter, it was improved to 5.71 dBi from 5.2 dBi without affecting the bandwidth. Ant. 5, the proposed design, incorporates additional slits, each with a depth of 4 mm, into the patch and presented in Fig. 2(e). The suggested configuration provides a bandwidth of 2 GHz and a high gain of 6.25 dBi with a reflection coefficient of  $-43.82$  GHz at an operating frequency of 16.9 GHz. Fig. 3 shows simulated  $S_{11}$  values for the evaluation steps of antenna configuration, also listed in Table 2 for each iteration process (Ant. 1 to Ant. 5).

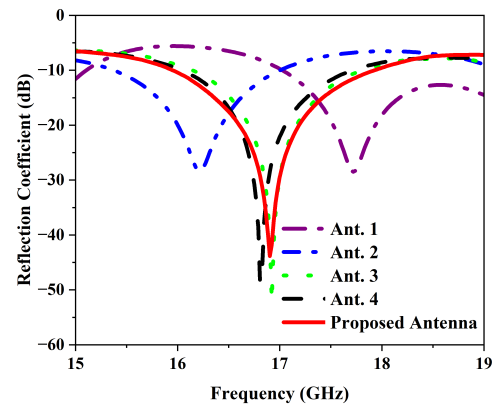


FIGURE 3. Time division process for radar and communication.

## 2.2. Parametric Analysis

Figure 4 shows the analysis of the proposed antenna’s behavior, specifically delving into the impacts of  $R$ ,  $d_1$ , and  $K$ , meticulously examined using CST software.

### 2.2.1. Effect of Patch Radius ( $R$ )

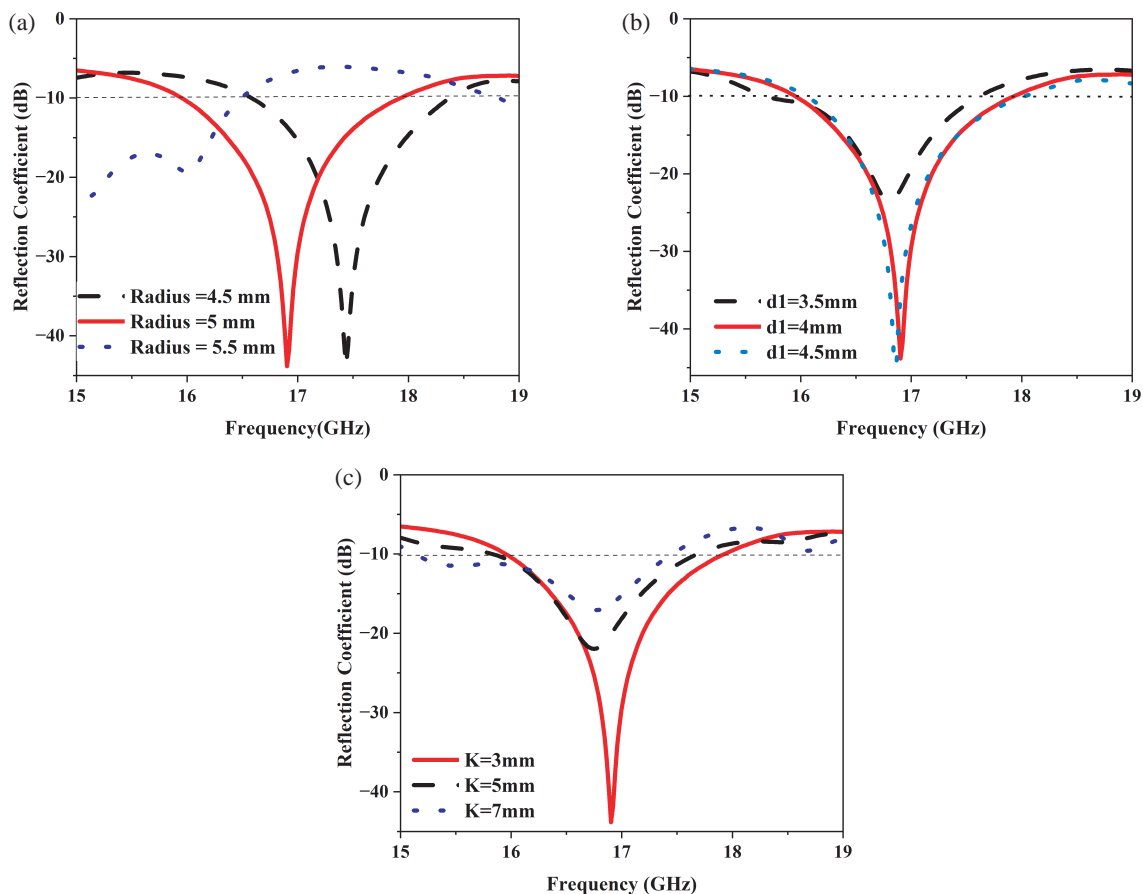
In Fig. 4(a), a parametric analysis explores various radius values. As  $R$  increases, the cutoff frequency shifts lower owing to the extended current path. Balancing bandwidth, gain, and reflection coefficient,  $R = 5$  mm was identified as the optimized value.

### 2.2.2. Effect of Slit Depth ( $d_1$ )

In Fig. 4(b), the  $S_{11}$  responses for varying values of slit depth ( $d_1$ ) are illustrated. The optimized value identified for the slit depth is 4 mm. From the simulation, it was observed that, for the depths of 4 mm and 4.5 mm, the reflection coefficients are close. However, the gain parameter value for the depth of 4 mm is 6.25 dBi, whereas for the depth of 4.5 mm it was noticed as 5.08 dBi with the same reflection coefficient and bandwidth. Balancing bandwidth, gain, and reflection coefficient,  $d_1 = 4$  mm was identified as the optimized value.

**TABLE 2.** Antenna parameters at different stages of antenna design.

Design	Operating frequency (GHz)	Reflection Coefficient, $S_{11}$ (dB)	Bandwidth (GHz)	Gain (dBi)
Ant. 1	17.72	-28.5	1.378	—
Ant. 2	16.219	-28.47	1.64	5.7
Ant. 3	16.922	-52.03	1.675	5.2
Ant. 4	16.808	-48.87	1.725	5.71
Proposed Antenna	16.903	-43.85	2.027	6.25

**FIGURE 4.** Reflection coefficient for different values of (a) patch radius —  $R$ , (b) slits depth —  $d_1$ , and (c) ground separation —  $K$ .

### 2.2.3. Effect of Ground Separation ( $K$ )

In designing the proposed antenna, the ground features two fractal defective ground structures, crucial for achieving notable antenna parameters. The positioning of these etched slots significantly impacts antenna performance. Therefore, an analysis was conducted to observe the impact of separation between the two fractal slots using CST. In Fig. 4(c), the reflection coefficient values are depicted across various separations from edge to edge of the slots. The simulated outcomes revealed that as the separation between the slots increased, the parameter values deteriorated.

## 3. SIMULATION RESULTS

The measurement setup in an anechoic chamber and vector network analyzer (VNA) results is also presented in Figs. 5(a) and (b) for validating the results.

### 3.1. S-Parameter Results

Figure 5(c) shows a comparison result between the simulated and measured reflection coefficients ( $S_{11} = S_{22}$ ). CST Microwave Studio shows that an open bandwidth is 2.02 GHz (15.946 to 17.973 GHz) for simulation at resonance frequency of 16.903 GHz with  $S_{11}$  being -43.82 dBi. The measured one

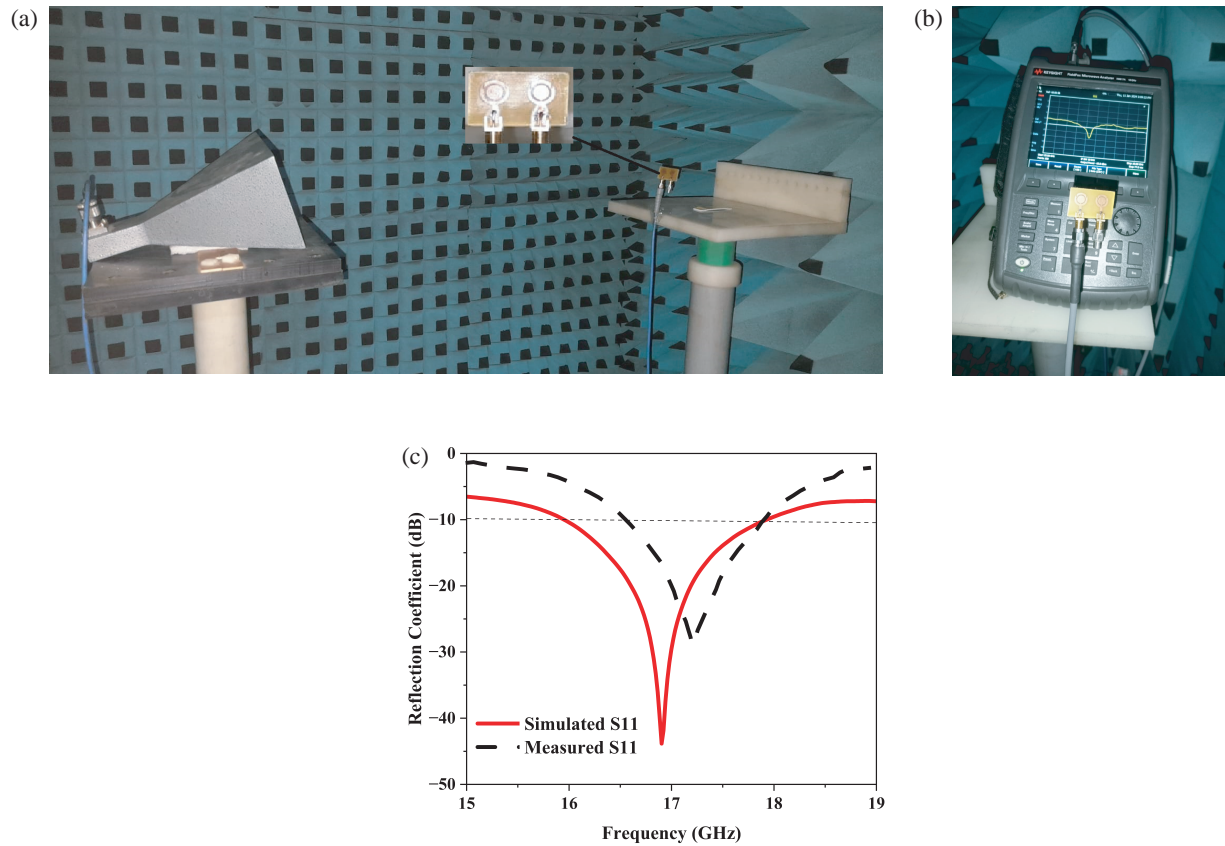


**FIGURE 5.** (a) The measurement setup in anechoic chamber. (b) Reflection coefficient in vector network analyser. (c) Simulated and Measured Reflection Coefficient.

is 1.327 GHz (15.946 to 17.973 GHz) measured at resonance frequency of 17.1 GHz with  $S_{11}$  being  $-28$  dBi. The small deviation is observed in the shifting of resonance frequency, i.e., 0.197 GHz. However, a good agreement in the comparison of the simulated and measured results has been observed of the proposed antenna.

### 3.2. Radiation Pattern

The measured and simulated results of radiation patterns cross polarization (X-Pol) and co-polarization (Co-Pol) for  $E$ -plane and  $H$ -plane are shown in Figs. 6(a) and 6(b) at 16.903 GHz of the resonance frequency of the proposed antenna. A good agreement in the comparison of the simulated and measured results has been observed. Fig. 6(c) shows the obtained 3D gain plot at 16.903 GHz as 6.25 dBi. These results are suitable for satellite communications, particularly in downlink applications, enabling faster data transmission rates.

### 3.3. Surface Current Distributions

Surface current in antennas signifies the flow of current along the surface of an antenna element, particularly when the dimensions closely match the wavelength of the electromagnetic wave that they transmit or receive. However, accounting for surface current enables simplification in analysis. Figs. 7(a)

and 7(b) depict the surface current distributions at the operating frequency when both ports are excited independently.

### 3.4. Envelope Correlation Coefficient (ECC) and Diversity Gain (DG)

For optimal pattern diversity in utilizing antenna elements, a fundamental necessity is for their radiation patterns to exhibit minimal correlation. The measurement employed to assess the correlation between radiation patterns is termed as envelope correlation coefficient (ECC). In MIMO applications, ECC can be computed using either the far-field radiation pattern or scattering parameter approach. Calculating the ECC parameter from 3D far-field radiation pattern measurements is ideal, but it can become intricate and laborious. Therefore, ECC calculations based on  $S$ -parameters are preferred and prioritized. ECC between elements  $i$  ( $i = 1$ ) and  $j$  ( $j = 2$ ) can be computed from scattering parameters using the following Equation (3) [16]:

$$ECC_{ij} = \frac{|S_{ii}^* S_{ij} + S_{ji}^* S_{jj}|^2}{[1 - (|S_{ii}|^2 + |S_{ji}|^2)][1 - (|S_{jj}|^2 + |S_{ij}|^2)]} \quad (3)$$

$$Diversity\ Gain\ (DG) = 10\sqrt{1 - |ECC_{ij}|^2} \quad (4)$$

The  $S$ -parameter approach yields ECC values below 0.025 and DG values exceeding 9.89 dB derived from Equation (4). Normalized ECC and diversity gain graphical representation are

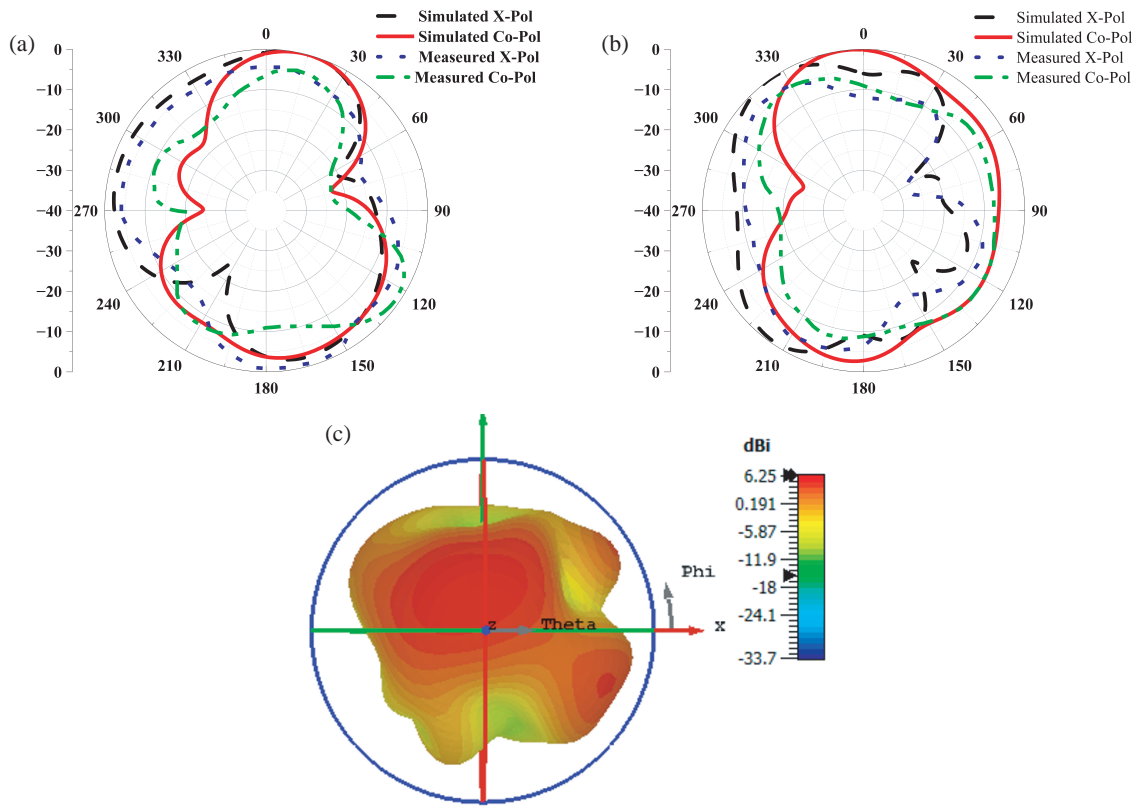


**FIGURE 6.** Simulated and Measured Cross Pol and Co-Pol of (a) *E*-Plane, (b) *H*-Plane at 16.903 GHz, (c) 3D Gain Plot for proposed two port MIMO antenna.

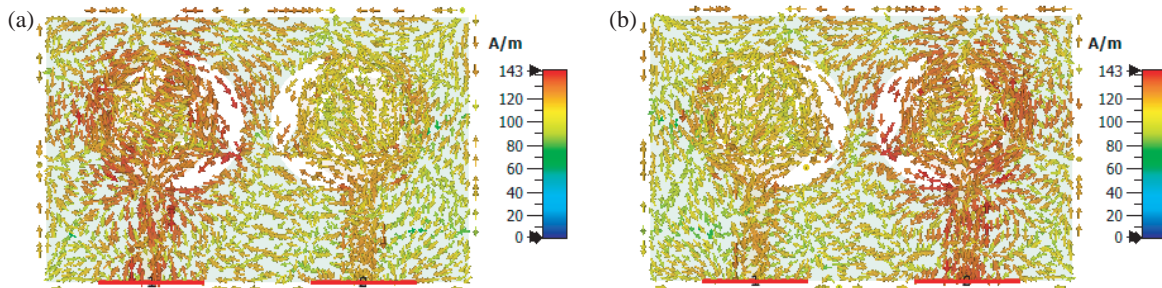


**FIGURE 7.** Surface currents at 16.903 GHz (a) when port 1 is excited, (b) when port 2 is excited.

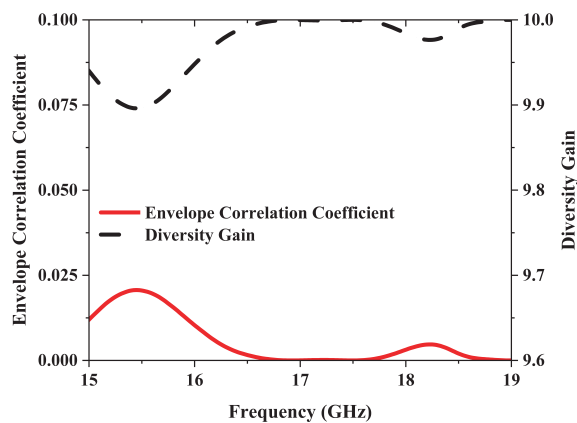


**FIGURE 8.** ECC and Diversity Gain plot of the proposed antenna.

**TABLE 3.** Comparative study of the proposed antenna.

Ref. No	Substrate Material	Resonating Frequency (GHz)	Bandwidth (GHz)	Gain (dBi)	Antenna Dimensions (mm <sup>2</sup> )	Applications
[2]	FR-4	13.67 15.28	0.854 1.14	8.01 6.01	40 × 48	Satellite Communication
[3]	Silicon Spacer	1.91 2.21	0.62	9.37	80 × 50	Wireless Communication
[4]	FR-4	6.6 9.4	0.41 0.4	4.77 6.29	26 × 32	Satellite and Radar
[7]	RT Durioid 5880	4.19 8.79 13	0.43 0.4 1.0	5.01 5.42 7.46	82 × 64	Wireless Applications
[11]	FR4	0.94 1.94 2.47	0.25 0.4 0.26	5.8 6.5 6.5	130 × 150	Mobile Communications
[12]	FR4	2.45 5.5	0.65 0.975	2.6 3.8	50 × 50	WLAN
[14]	FR-4	2.5 6.4	0.83 2.37	3.10 3.58	50 × 32	5G Communications
Proposed Antenna	FR-4	16.9	2.027	6.25	20 × 32	Satellite Communication

presented in Fig. 8. In Table 3, the comparisons of existing antennas to the proposed antenna are summarized. It is observed that the bandwidth and gain are more, and the size of the proposed antenna is less.

#### 4. CONCLUSION

This paper highlights a compact, high-gain circular two-port MIMO antenna with fractal DGS designed for downlink applications in satellite communication. Employing slits, slots, and fractal DGS enables the attainment of wideband capability and high gain, both essential for effective satellite communication applications. The measurements of the recommended antenna are compact, measuring  $20 \times 32 \times 1.62 \text{ mm}^3$ . The designed antenna offers a wideband at a resonating frequency of 16.903 GHz with a reflection coefficient of  $-43.82 \text{ dB}$  and isolation between the elements of  $< -15 \text{ dB}$ . The impedance bandwidth at the reflection coefficient is 2.027 GHz, observed with a gain of 6.25 dBi. Far-field characteristics of the  $E$ -plane and  $H$ -plane were observed at resonating frequencies. To confirm the diversity performance, simulated results demonstrate ECC (below 0.025) and diversity gain (above 9.89).

#### ACKNOWLEDGEMENT

This work was supported by the SERB, Department of Science and Technology (DST), New Delhi, India. (Grant No. 1: SB/FTP/ETA-0179/2014, Grant No. 2: EEQ/2016/000754.)

#### REFERENCES

- [1] Garg, R., *Microstrip Antenna Design Handbook*, Artech House, 2001.
- [2] Naik, K. K. and P. A. V. Sri, "Design of hexadecagon circular patch antenna with DGS at Ku band for satellite communications," *Progress In Electromagnetics Research M*, Vol. 63, 163–173, 2018.
- [3] Islam, M. T., M. N. Shakib, and N. Misran, "Broadband E-H shaped microstrip patch antenna for wireless systems," *Progress In Electromagnetics Research*, Vol. 98, 163–173, 2009.
- [4] Kumar Naik, K. and P. A. V. Sri, "Design of concentric circular ring patch with DGS for dual-band at satellite communication and radar applications," *Wireless Personal Communications*, Vol. 98, 2993–3001, 2018.
- [5] Elftouh, H., N. A. Touhami, M. Aghoutane, S. E. Amrani, A. Tazón, and M. Boussouis, "Miniaturized microstrip patch antenna with defected ground structure," *Progress In Electromagnetics Research C*, Vol. 55, 25–33, 2014.
- [6] Werner, D. H. and S. Ganguly, "An overview of fractal antenna engineering research," *IEEE Antennas and Propagation Magazine*, Vol. 45, No. 1, 38–57, 2003.
- [7] Naik, K. K., G. Dattatreya, R. P. S. Chaitanya, R. Palla, and S. S. Rani, "Enhancement of gain with corrugated Y-shaped patch antenna for triple-band applications," *International Journal of RF and Microwave Computer-Aided Engineering*, Vol. 29, No. 3, e21624, 2019.
- [8] Ullah, S., C. Ruan, M. S. Sadiq, T. U. Haq, A. K. Fahad, and W. He, "Super wide band, defected ground structure (DGS), and stepped meander line antenna for WLAN/ISM/WiMAX/UWB and other wireless communication applications," *Sensors*, Vol. 20, No. 6, 1735, 2020.

- [9] Wei, F., L. Chen, X.-W. Shi, and C.-J. Gao, "UWB bandpass filter with one tunable notch-band based on DGS," *Journal of Electromagnetic Waves and Applications*, Vol. 26, No. 5-6, 673–680, 2012.
- [10] Sharma, P., R. N. Tiwari, P. Singh, P. Kumar, and B. K. Kanaujia, "MIMO antennas: Design approaches, techniques and applications," *Sensors*, Vol. 22, No. 20, 7813, 2022.
- [11] Bayatmaku, N., P. Lotfi, M. Azarmanesh, and S. Soltani, "Design of simple multiband patch antenna for mobile communication applications using new E-shape fractal," *IEEE Antennas and Wireless Propagation Letters*, Vol. 10, 873–875, 2011.
- [12] Peng, H., R. Zhi, Q. Yang, J. Cai, Y. Wan, and G. Liu, "Design of a MIMO antenna with high gain and enhanced isolation for WLAN applications," *Electronics*, Vol. 10, No. 14, 1659, 2021.
- [13] Ren, J., W. Hu, Y. Yin, and R. Fan, "Compact printed MIMO antenna for UWB applications," *IEEE Antennas and Wireless Propagation Letters*, Vol. 13, 1517–1520, 2014.
- [14] Babu, K. V., P. S. Rao, B. C. Naik, and B. R. Kumar, "Compact dual-band design and analysis of half-circular U-shape MIMO radiator for wireless applications," *Microsystem Technologies*, Vol. 29, No. 4, 501–514, 2023.
- [15] Mia, M. M., M. S. Islam, M. F. Ahmed, M. H. Kabir, M. A. Islamand, and M. M. Islam, "Design of aminiature rectangular patch antenna for KU band applications," *The International Journal of Ambient Systems and Applications*, Vol. 10, No. 4, 01–07, 2022.
- [16] Ghosh, B., S. K. M. Haque, and D. Mitra, "Miniaturization of slot antennas using slit and strip loading," *IEEE Transactions on Antennas and Propagation*, Vol. 59, No. 10, 3922–3927, 2011.
- [17] Dastranj, A., A. Imani, and M. Naser-Moghaddasi, "Printed wide-slot antenna for wideband applications," *IEEE Transactions on Antennas and Propagation*, Vol. 56, No. 10, 3097–3102, 2008.
- [18] Qin, P.-Y., F. Wei, and Y. J. Guo, "A wideband-to-narrowband tunable antenna using a reconfigurable filter," *IEEE Transactions on Antennas and Propagation*, Vol. 63, No. 5, 2282–2285, May 2015.
- [19] Naik, K. K., "Improvement of wider bandwidth using dual E-shaped antenna for wireless communications in 5G applications," *Analog Integrated Circuits and Signal Processing*, Vol. 109, No. 1, 93–101, 2021.
- [20] Ketavath, K. N., "Enhancement of gain with coplanar concentric ring patch antenna," *Wireless Personal Communications*, Vol. 108, No. 3, 1447–1457, 2019.
- [21] Asci, Y., "Wideband and stable-gain cavity-backed slot antenna with inner cavity walls and baffle for X-and Ku-band applications," *IEEE Transactions on Antennas and Propagation*, Vol. 71, No. 4, 3689–3694, 2023.
- [22] Bilgic, M. M. and K. Yegin, "Wideband offset slot-coupled patch antenna array for X/Ku-band multimode radars," *IEEE Antennas and Wireless Propagation Letters*, Vol. 13, 157–160, 2014.
- [23] Liu, L., S. W. Cheung, and T. I. Yuk, "Compact MIMO antenna for portable devices in UWB applications," *IEEE Transactions on Antennas and Propagation*, Vol. 61, No. 8, 4257–4264, 2013.
- [24] Saxena, S., B. K. Kanaujia, S. Dwari, S. Kumar, and R. Tiwari, "MIMO antenna with built-in circular shaped isolator for sub-6 GHz 5G applications," *Electronics Letters*, Vol. 54, No. 8, 478–480, 2018.
- [25] Addepalli, T. and V. R. Anitha, "A very compact and closely spaced circular shaped UWB MIMO antenna with improved isolation," *AEU — International Journal of Electronics and Communications*, Vol. 114, 153016, 2020.